Position preference and diffusion path of an oxygen ion in apatite-type lanthanum silicate La9.33Si6O26: a density functional study

Abstract

Using density functional theory, we investigated the position preference and diffusion mechanisms of interstitial oxygen ions in lanthanum silicate $La_{9.33}Si_6O_{26}$, which is an apatite-structured oxide and a promising candidate electrolyte material for solid oxide fuel cells. The reported lanthanum vacancies were explicitly taken into account by theoretically determining their arrangement with a supercell model. The most stable structures and the formation energies of oxygen interstitials were determined for each charged state. It was found that the double-negatively charged state is stable over a wide range of the Fermi level, and that the excess oxygen ions form split interstitials with the original oxygen ions, while the neutral and the single-negatively charged states preferably form molecular oxygen. These species were found near the lanthanum vacancy site. The theoretically determined migration pathway along the *c*-axis essentially follows an interstitialcy mechanism. The obtained migration barrier is sensitive to the charge state, and is also affected by the lanthanum vacancy. The barrier height of the double-negatively charged state was calculated to be 0.58 eV for the model structure, which is consistent with the measured activation energy.

Keywords

study, preference, functional, position, density, 33si6o26, la9, silicate, lanthanum, type, apatite, ion, oxygen, path, diffusion

Disciplines

Engineering | Physical Sciences and Mathematics

Publication Details

Liao, T, Sasaki, T, Suehara, S & Sun, Z (2011), Position preference and diffusion path of an oxygen ion in apatite-type lanthanum silicate La9.33Si6O26: a density functional study, Journal of Materials Chemistry, 21(9), pp. 3234-3242.

Journal of Materials Chemistry

Cite this: *J. Mater. Chem.*, 2011, **21**, 3234

www.rsc.org/materials

PAPER

Position preference and diffusion path of an oxygen ion in apatite-type lanthanum silicate $La_{9.33}Si_6O_{26}$: a density functional study

Ting Liao,†[a] Taizo Sasaki,*[ab] Shigeru Suehara[a] and Ziqi Sun[c]

Received 30th July 2010, Accepted 25th November 2010
DOI: 10.1039/c0jm02473b

Using density functional theory, we investigated the position preference and diffusion mechanisms of interstitial oxygen ions in lanthanum silicate $La_{9.33}Si_6O_{26}$, which is an apatite-structured oxide and a promising candidate electrolyte material for solid oxide fuel cells. The reported lanthanum vacancies were explicitly taken into account by theoretically determining their arrangement with a supercell model. The most stable structures and the formation energies of oxygen interstitials were determined for each charged state. It was found that the double-negatively charged state is stable over a wide range of the Fermi level, and that the excess oxygen ions form split interstitials with the original oxygen ions, while the neutral and the single-negatively charged states preferably form molecular oxygen. These species were found near the lanthanum vacancy site. The theoretically determined migration pathway along the *c*-axis essentially follows an interstitialcy mechanism. The obtained migration barrier is sensitive to the charge state, and is also affected by the lanthanum vacancy. The barrier height of the double-negatively charged state was calculated to be 0.58 eV for the model structure, which is consistent with the measured activation energy.

1. Introduction

The solid oxide fuel cell (SOFC) is a wide-temperature-range (500–1000°C) electrochemical device that utilizes hydrogen or hydrocarbons as an anode fuel. The SOFC has become a viable replacement for existing power sources due to its high energy conversion efficiency, fuel flexibility that may allow direct operation on natural gas, and environmental safety.[1] Recent progress in SOFCs can be partly attributed to the development of new electrolyte materials, which are a key component of the electrochemical cell.[2]

Among the novel oxygen ionic conductors reported in the recent literature, apatite-structured lanthanum silicates have been of great interest because of their high ionic conductivity, low electronic conductivity, intermediate operational temperature range, and moderate thermal expansion coefficients.[3] For example, an electrochemical cell with an apatite-type $La_{10}Si_{5.5}Al_{0.5}O_{26.75}$ electrolyte was recently re-evaluated.[4] This material has a higher conductivity than yttria-stabilized zirconia, and is comparable to most of the solid electrolytes proposed for the intermediate temperature range, such as doped ceria and lanthanum gallate-based electrolytes.

Lanthanum silicate $La_{9.33}Si_6O_{26}$ has the $P6_3/m$ space group[5,6] and belongs to a general class of 'apatite' compounds (Fig. 1). These compounds contain compact tetrahedral 'anion' structural units $(SiO_4)^{4-}$ with strong covalent bonding, which are networked with each other to produce higher-coordination sites such as nine-coordinated and trigonal bi-pyramidal sites that are occupied by lanthanum ions. The former is (1/3, 2/3, *z*) 4*f* in the

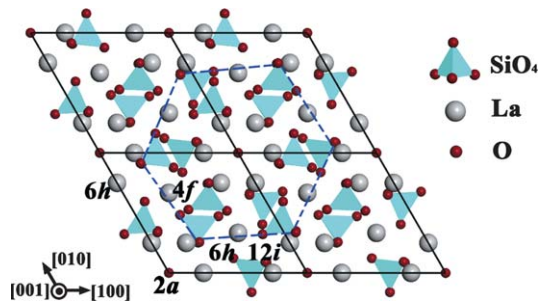

Fig. 1 The apatite structure of $La_{9.33}Si_6O_{26}$. The atoms in different Wyckoff positions are labeled accordingly in one of the unit cells. The atomic environment encompassing the conduction channel used to illustrate the oxygen interstitial position in Fig. 4 is indicated by dashed lines.

[a]*Computational Materials Science Center (CMSC), National Institute for Materials Science, 1-2-1 Sengen, Tsukuba, Ibaraki, 305-0047, Japan. E-mail: SASAKI.Taizo@nims.go.jp; Fax: +81-29-859-2601; Tel: +81-29-859-2618*
[b]*Innovative Center of Nanomaterials Science for Environment and Energy (ICNSEE), National Institute for Materials Science, 1-2-1 Sengen, Tsukuba, Ibaraki, 305-0047, Japan*
[c]*WPI International Center for Materials Nanoarchitectonics (MANA), National Institute for Materials Science, 1-1 Namiki, Tsukuba, Ibaraki, 305-0044, Japan*
† Present address: Australian Institute of Bioengineering and Nanotechnology (AIBN), Building #75, The University of Queensland, St. Lucia, QLD4072, Australia.

Wyckoff notation, and the latter is (x, y, 1/4) 6h. These sites, however, necessarily contain vacancies because of the non-stoichiometric La content, and structural analysis has indicated that these are limited to the 4f sites. The framework formed by $(SiO_4)^{4-}$ units and La ions at the 6h sites circumscribes a [001] hexagonal channel.

As with virtually all ionic conductors, the properties of $La_{9.33}Si_6O_{26}$, and therefore its performance, are defect sensitive. Previous studies[7] of oxygen conduction/diffusion in the $La_{9.33}Si_6O_{26}$ system have supported the idea that the oxygen interstitial (O_i) is the dominant charge carrier, instead of the usual oxygen vacancy. Thus, the concentration of O_i controls the transport properties of these electrolytes. A migration mechanism of O_i in $La_{9.33}Si_6O_{26}$ has been proposed on the basis of atomistic simulations. Using modified interatomic potentials, Tolchard *et al.*[8] found that the oxygen ionic conduction/diffusion adopts a non-linear (sinusoidal-like) pathway through the stable position near the edge of the open channel. Recently, a new oxygen interstitial configuration and a migration mechanism with a lower migration barrier in $La_{9.33}Si_6O_{26}$ were proposed by Béchade *et al.*[9] on the basis of a similar atomistic simulation technique.

Despite these achievements, and to clarify the ambiguities, a thorough and precise understanding of the most stable configuration and the migration mechanism of oxygen defects at an electronic level for apatite oxide-ion conductors is required. In addition, the lanthanum vacancy (V_{La}) is expected to introduce a large inhomogeneity in the potential energy of defects, since the electrostatic potential will be less screened by electrons than in metals. However, the role of V_{La} in the diffusion of O_i has not been sufficiently considered. For example, if the inhomogeneity creates a trap for the diffusing species, the migration barrier would be primarily determined by its depth. In the present system, since the oxygen atom is assumed to migrate in a one-dimensional channel, the effect of the inhomogeneity could be significant in the migration.

In this study, we examined the oxygen ionic conduction mechanism in $La_{9.33}Si_6O_{26}$ using the extensively employed density-functional theory. We determined (i) the electronic structure of $La_{9.33}Si_6O_{26}$, (ii) the most stable geometry and formation energy of O_i, and (iii) the migration path and energy barrier of O_i, explicitly considering the effects of the charge state and the relative geometry to the preexisting V_{La}. The results will be presented and discussed after a description of the theoretical details.

2. Theoretical scheme

Total energy calculations were carried out within the density functional theory (DFT) with the generalized gradient approximation (GGA) in the Perdew-Burke-Emzerhof form.[10] The electron-core interaction was represented by the ultrasoft pseudopotential method.[11] The psedopotentials were generated by the reference configuration of $2s^2$ and $2p^4$ for O, $3s^2$ and $3p^2$ for Si, and $5s^2$, $5p^6$, $5d^1$, $6s^{1.5}$, and $6p^{0.5}$ for La. Plane waves of which kinetic energy is less than 50 Ry were used as basis functions for the wave functions, and 200 Ry for the charge density distribution. The error due to these cut-off energies was 2.0×10^{-4} eV per cell.

Lattice constants and internal positions in perfect unit cells were fully optimized until all residual Hellmann-Feynman forces on each atom and residual stresses were reduced to within 10^{-3} Ry Bohr^{-1} (2.6×10^{-2} eV Å^{-1}) and 0.05 GPa, respectively. The k-point mesh for the Brillouin zone integration was selected according to the Monkhorst–Pack scheme.[12] The numerical calculations were performed using the PWSCF code.[13]

A supercell was constructed for the calculation of $La_{9.33}Si_6O_{26}$ and for systems with excess oxygen. The size of the supercell was chosen to be $1 \times 1 \times 3$ times the conventional apatite unit cell, amounting to 124 (+1) atoms. This was the minimum practical size for the explicit modeling of V_{La}. Throughout present paper, atomic coordinates in the supercell are expressed in units of the lattice constant of the conventional cell. A $2 \times 2 \times 2$ shifted k-point mesh was adopted for the total energy calculation. In the charged defect calculations, a specific charge was assigned to the supercell. A neutralizing homogeneous background charge was assumed in order to avoid divergence of the long-range interactions between the defect and its periodic images. No further correction for this interaction was included in the present calculations since there is an ambiguity on screening of the defect potential by the surrounding electrons and ion clusters.

The formation enthalpy $E_f[X_q]$ of defect species X in charge state q is given by,[14]

$$E_f[X^q] = E_{tot}[X^q] - E_{tot}[\text{bulk}] - \sum_i n_i\mu_i + q\left[E_F + E_v + \Delta V_q\right], \quad (1)$$

where E_{tot}[bulk] and $E_{tot}[X_q]$ are the total energies of the perfect and defect-containing supercells, respectively, and μ_i and n_i are the chemical potential and the number of the i-th atom, respectively. E_F is the Fermi level, measured from the top of the valence band (valence band maximum, VBM) E_v. For consistency in the total energies of a charged defect and of the perfect cell, the potentials were aligned by ΔV_q in eqn(1), which was estimated from the energy bands localized at atoms away from the defect center.

It should be noted that spin polarization is necessary for precise estimation of the energy of the open shell case in DFT, such as that of a single negatively-charged oxygen interstitial. In our case, however, the spin polarization was found to not significantly affect the stability of the charged states, and the energy reduction due to the spin polarization was only 0.036 eV in the total energy of the stable geometry.

The nudged elastic band (NEB) method[15] was used to find the migration paths and to evaluate potential barriers on these paths. In the migration path search, all conditions were the same as in the total energy calculation of the supercell except for the k-point sampling, in which only the Γ point was used. In order to estimate the error caused by the smaller sampling, calculations of all oxygen interstitial migration barriers with a k-point sampling at the M point (0, 1/2, 0), but not at the Γ point, were performed separately. The difference in the resulting migration energies was within 0.005 eV.

3. Results and discussion

3.1 Crystal and electronic structure of $La_{9.33}Si_6O_{26}$

Prior to carrying out the supercell calculations to model oxygen interstitials, energy minimization of the original $La_{9.33}Si_6O_{26}$

lattice was performed to generate the equilibrium structure. Since the current content of the lanthanum silicate in the apatite-type structure assumes V_{La}s, their configuration and energetics were explored first. Previous experimental results indicated that V_{La}s reside at the 4*f* La sites. To determine a distribution of V_{La}s and minimize structural distortion, four different arrangements of V_{La}s in opposing columns of the 1 × 1 × 3 supercell were examined to find the most stable configuration of the host $La_{9.33}Si_6O_{26}$ lattice and address any possible vacancy-vacancy interactions. The examined La vacancy arrangements are indicated as the *n*-th nearest neighbors to a preexisting V_{La}.

To better understand the V_{La} arrangement in our specified supercell, we mapped the relevant interaction energies between V_{La}s in Fig. 2, which was obtained from the total energies of independent V_{La}s and the no-vacancy lattice. It can be seen that the arrangement denoted as 4NN was predicted to be the most favorable of these configurations. The results also indicate that the interaction between the vacancies is repulsive, even for 3NN. Therefore, the vacancies should tend to be distributed uniformly. Experimentally, there is no evidence of an ordered arrangement of V_{La}s. The random distribution of V_{La} is probably a quenched structure that is dependent upon the sample preparation conditions. We assumed the 4NN configuration of V_{La} in the present calculations. We also note that for the excess-La case, the atoms tend to distribute uniformly because of the positive interaction energy values.

Calculated and experimental lattice constants and formation enthalpies ΔE_f of $La_{9.33}Si_6O_{26}$ and binary oxides, SiO_2 (α-quartz) and La_2O_3, are summarized in Table 1. It can be seen that the GGA calculations reproduced the experimentally-determined structural parameters of $La_{9.33}Si_6O_{26}$ with errors of less than 0.6%. The deviations of the calculated internal atomic coordinates from the experimental values are also within 1.0%, but are not listed in the table. The calculated formation energies were underestimated in absolute value, compared to the experimental values. Such deviations have often been observed in GGA calculations for oxides, and an explanation associating it with the error in the ionization energy of an oxygen atom has been proposed.[16]

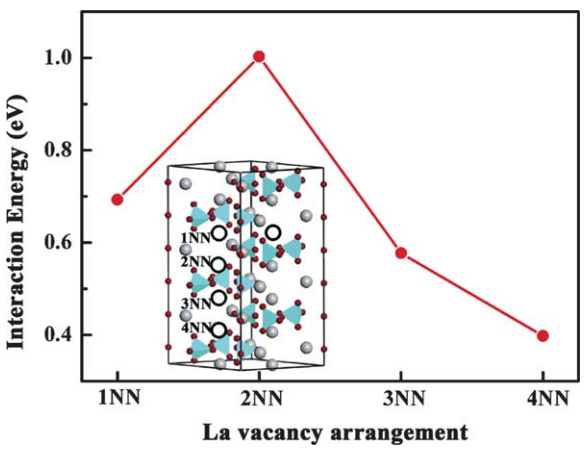

Fig. 2 Lanthanum vacancy interaction energies as a function of lanthanum vacancy spacing: *n*NN (*n* = 1, 2, 3, and 4) denotes a lanthanum vacancy at the *n*-th-nearest spacing to the preexisting lanthanum vacancy. The finite $La_{9.33}Si_6O_{26}$ supercell used is shown in the inset.

Fig. 3 exhibits the total and electronic projected density of states (total DOS and PDOS) for $La_{9.33}Si_6O_{26}$. PDOS is obtained by projecting the wavefunctions onto the orthogonalized atomic wavefunctions. The calculated total DOS indicated that the energy gap E_{gap} of $La_{9.33}Si_6O_{26}$ is 4.87 eV, indicating electronically insulating properties, as expected from the nominal ionic valence. It should be noted that GGA is known to underestimate the energy gap by 50% or more, generally. Although the present result seems to underestimate the gap, there is insufficient experimental data on the band structure of $La_{9.33}Si_6O_{26}$ for a proper comparison.

The PDOS analysis in Fig. 3 indicates that the highest valence band is formed mainly by the O-2p orbitals, hybridized with components of the surrounding cations. In the relatively lower energy region from around −7.0 to −3.0 eV, the valence band consists of the O-2p orbitals at 6*h* and 12*i* sites hybridized with the 3s/3p component of Si and a partial contribution from the La-5d orbitals. The O-2p orbital at the 2*a* site is distributed over a higher energy range from −5.0 eV to the VBM, along with some components of the La-5d orbitals. As noticed in Fig. 3, the bottom of the conduction band (the conduction band minimum, CBM) is mainly composed of the La-5d orbital.

3.2 Fermi-level-tuned oxygen interstitial position

In order to find the most energetically stable excess-oxygen atomic configurations, different inserted positions, from the conduction channel center to its periphery, and different symmetric arrangements were carefully examined, including the interstitial positions reported experimentally and theoretically for several of the charged states. The obtained equilibrium geometries are displayed in Fig. 4. Both the neutral and single-negatively charged oxygen interstitial ($O_i^{\times}$ and O'_i in the Kröger-Vink notation) have configurations characterized by a linear arrangement of an oxygen interstitial pair along the [001] direction in the conduction channel center. This arrangement is formed when an inserted oxygen atom pushes a second oxygen atom in the 2*a* position away, placing their midpoint on the original lattice site. The equilibrium interatomic distances of the split oxygen atoms for $O_i^{\times}$ and O'_i are 1.520 Åand 2.175 Å, respectively. While the displacement of the surrounding atoms caused by $O_i^{\times}$ is quite small, despite the split pair formation, no bigger than 0.1 Å. O'_i causes larger local distortion: The maximum displacement (0.247 Å on average) occurrs at the 2*a*-site oxygen atoms neighboring the split pair.

In the case of the double-negatively-charged oxygen interstitial (O''_i), as illustrated in Fig. 4 (c), the lowest energy oxygen interstitial configuration is also the split interstitial, but its midpoint is not at the channel center and the split pair axis is aligned in the [012] direction. The calculated equilibrium positions are (−0.0820, −0.0964, 0.6093) and (0.0117, 0.1051, 0.9144), which are separated by 2.787 Å. The observed distortion has long-range characteristics with relatively large displacements (0.15–0.56 Å), including La atoms (6*h*-site) neighboring each O atom in the pair and surrounding O atoms (2*a*-, 6*h*-, and 12*i*-sites). The most stable configuration obtained by Béchade *et al.*[9] with atomistic simulation was (−0.0883, −0.106, 0.588)

Table 1 Calculated and experimental lattice parameters and formation energy ΔE_f of $La_{9.33}Si_6O_{26}$ apatite 1 × 1 × 3 supercell, renormalized with respect to the equivalent unit cell, and for SiO_2 and Al_2O_3

	This work	Atomistic calculations	Experiments
$La_{9.33}Si_6O_{26}$			
a/Å	9.725	9.9089[c], 9.7607[f]	9.719[a], 9.7158[b], 9.7248[d], 9.71297[e]
c/Å	7.150	7.1659[c], 7.1178[f]	7.187[a], 7.1883[b], 7.1895[d], 7.17950[e]
ΔE_f (eV/f.u.)	−134.610		−151.314[g]
SiO_2			
a/Å	5.032		4.913
c/Å	5.523		5.405
ΔE_f (eV/f.u.)	−8.313	−8.36[h]	−9.45
La_2O_3			
a/Å	3.896	3.94[i]	3.939
c/Å	6.156	6.19[i]	6.136
ΔE_f (eV/f.u.)	−16.843	−17.62[i]	−18.568

[a] Data of Iwata *et al.*[17] [b] Data of León-Reina *et al.*[18] [c] Based on results of Béchade *et al.*[9] [d] Data of Sansom *et al.*[19] [e] Data of Matsushita *et al.*[6] [f] Based on results of Islam *et al.*[20] [g] Data of Risbud *et al.*[21] [h] Based on results of Detraux *et al.*[22] [i] Based on results of Kuwabara and Tanaka.[23]

and (0.0177, 0.106, 0.912), in which the crystal axes are converted, and both calculations agree to within 0.2 Å on the equilibrium position of the interstitial oxygen.

The present study assumed V_{La}s explicitly in the supercell, and their configurations were modeled as described in the previous section. Their positions with respect to the split pair position given above are (1/3, 2/3, 1/2) and (2/3, 1/3, 2). It follows that the split pair of excess oxygen resides near one of the vacancies. The pair's relationship with the vacancy will be discussed in the next section.

In the present calculations it was found that some stable interstitial positions in a specific charged state become less stable, or even unstable, when more electrons are inserted or removed. Other geometrical positions become stable, demonstrating charge-induced multistability in the $La_{9.33}Si_6O_{26}$ conductor. This is because these interstitial configurations are quite sensitive to the surrounding atomic bonding environment arising from local charges.

It is interesting to compare the interatomic distance of the neutral split interstitial pair with the atomic and ionic radii; twice the radius of the neutral oxygen atom is 1.2 Å, and twice the ionic radius is 2.76 Å. The separations of O_is in the neutral and single negatively charged states are between these two values. This indicates that a covalent bond is formed in the split pair. The separation between the O atoms in the double-negatively-charged pair is close to twice the ionic radii. In this case, the split

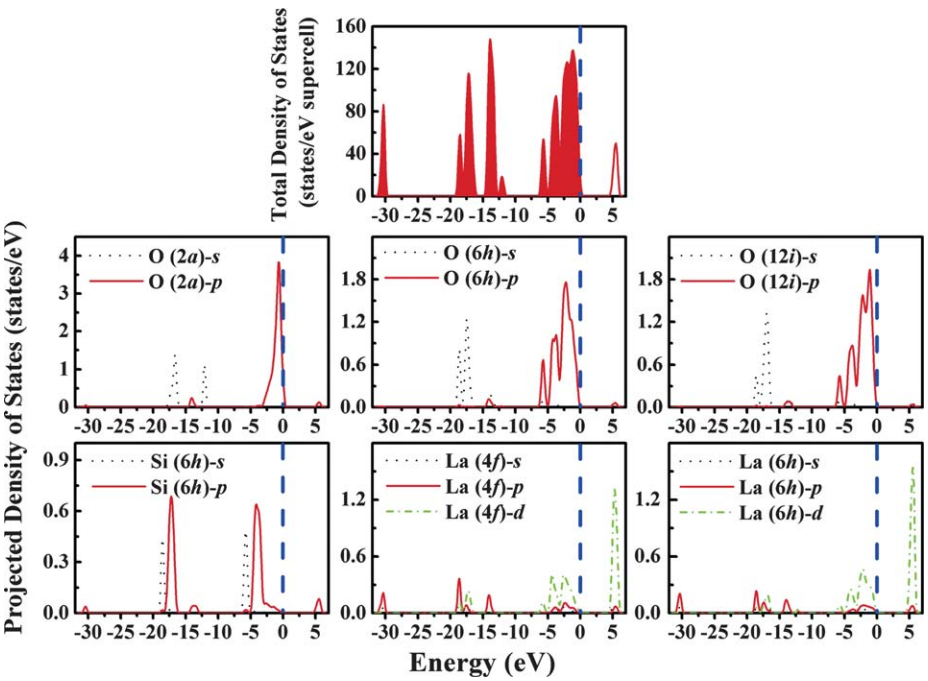

Fig. 3 Total and projected density of states for the host $La_{9.33}Si_6O_{26}$ lattice. Filled-in regions of the total DOS represent occupied states, and the top of the valence band is indicated by a vertical broken line.

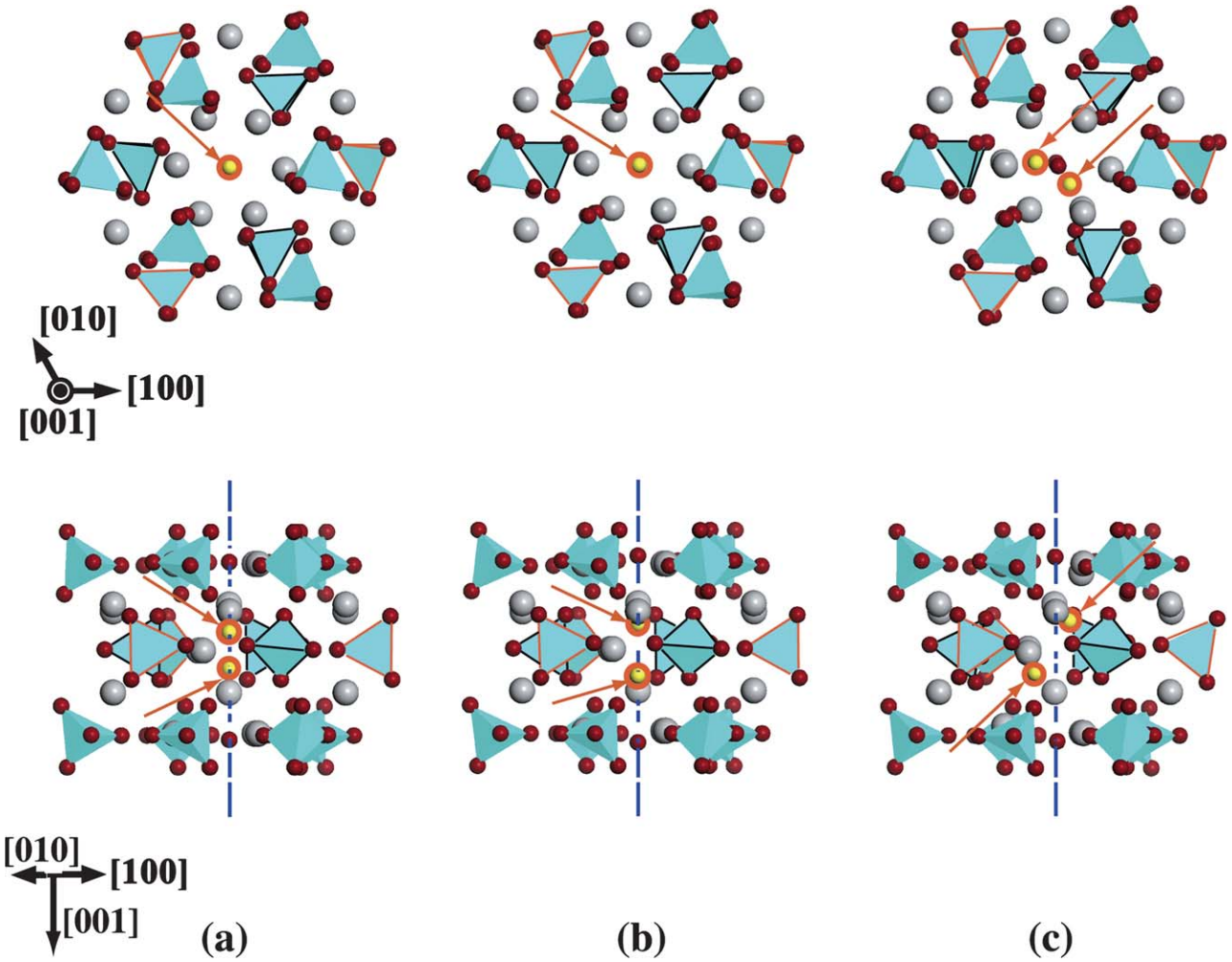

Fig. 4 Different views of the geometric structures of the lowest energy oxygen interstitial in $La_{9.33}Si_6O_{26}$: (a) neutral, (b) −1 charged, and (c) −2 charged states. The oxygen ions in the split pair are indicated by arrows.

pair consists of closely packed oxygen ions. We refer to the charge state as if it were for a single interstitial atom. The electron distribution, however, should be considered to extend over both atoms.

In materials with an energy gap, the Fermi level is a critical parameter in determining alternative defects and their charge states. The formation enthalpies of O_i with respect to the position of the Fermi level are presented in Fig. 5 (a).

Among all of the charged states considered, the full formal charge state is the most stable in a wide energy range of the Fermi level. The formation enthalpy of an oxygen Frenkel pair O''_i and $V_{\ddot{O}}$ in $La_{9.33}Si_6O_{26}$ was estimated from the energies of formation of a separated interstitial atom and a vacancy to be 3.83 eV. This value is quite large compared to the typical measured activation energy value for oxygen conduction of 0.4–0.8 eV.

The transition level $\varepsilon(q_1/q_2)$ can be defined as the Fermi level position at which the charge states q_1 and q_2 have equal formation energies.[24] $\varepsilon(O''_i/O'_i)$ and $\varepsilon(O'_i/O_i^{\times})$ have been obtained as 1.24 and 1.35 eV from comparison of the formation energies, respectively. Thus, the second acceptor level (O''_i/O'_i) is below the first acceptor level $(O'_i/O_i^{\times})$. This would correspond to a negative Coulomb parameter, and would make O'_i thermodynamically unstable. The transition levels of the charge states may be affected by the underestimation of the GGA gap. The effect of the gap underestimation has often been corrected in accordance with the following: if the one-electron states induced in the energy gap have a predominantly conduction-band character, they will likely shift upward with the conduction band when band-gap corrections are applied.[24] For valence-band derived states, the band-gap correction will only modestly affect the results. In the present results, the gap states were found to have the same character as that of the valence band, O-2p. Therefore, according to the above-mentioned consideration, the effect of the energy gap error should be small.

Fig. 6 shows the density of states projected on the O-2s and 2p orbitals of the two O atoms in a split interstitial as a blue shaded area, and the total DOS plotted as dot-dashed lines. The energy scales in Fig. 6 have been shifted to align the VBM with the reference energy of the model host $La_{9.33}Si_6O_{26}$ for comparison. When the excess oxygen is inserted, extra defect states are introduced into the energy gap, along with several common features in the valence band. Along with the incorporation of $O_i^{\times}$, the induced defect state in the energy gap is located near the CBM and remains unoccupied. In O'_i,

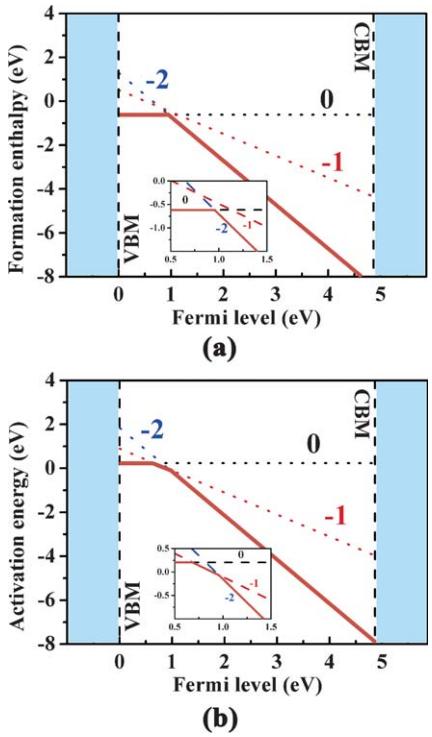

Fig. 5 Variation of (a) the formation enthalpies E_f and (b) the activation energies E_a ($=E_f + E_m$, where E_m is the migration barrier) of the oxygen interstitial as a function of the Fermi level under oxygen-rich conditions. The regions around the transition levels are expanded in the inset.

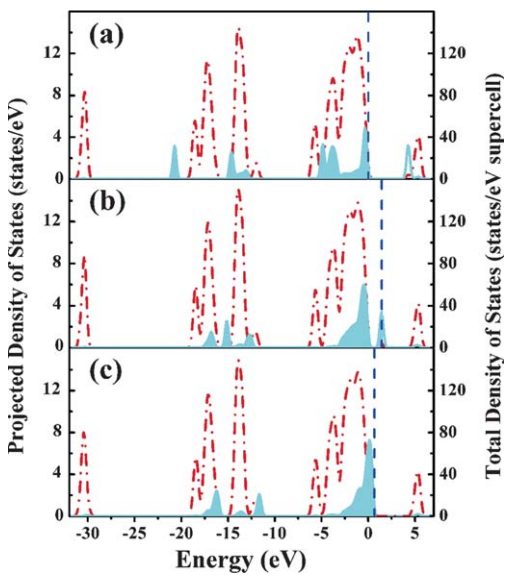

Fig. 6 Projected density of states at split-interstitial oxygen sites for (a) neutral, (b) −1, and (c) −2 charged states (the blue-shaded area corresponds to the left axis). The total DOS of each defective supercell is plotted as a dot-dashed line (which corresponds to the right axis). The VBM of ideal $La_{9.33}Si_6O_{26}$ was set to zero. The broken lines indicate the position of the highest occupied state.

half-occupied bands are observed deep in the band gap. The incorporation of O''_i introduces fully-occupied extra states near the VBM.

To provide additional insight into the charge distribution, and to help visualize the spatial distribution of the wave functions for the defect levels, we present a three-dimensional isosurface of the electron states in real space in Fig. 7. The isosurface of the one-electron states of the highest occupied and lowest unoccupied state are illustrated for the host and charged excess-oxygen supercells. For host $La_{9.33}Si_6O_{26}$, it is evident that the electronic states of the VBM are strongly localized at oxygen atoms at the 2*a* site with the spatial orientation of the O-2p orbitals aligned

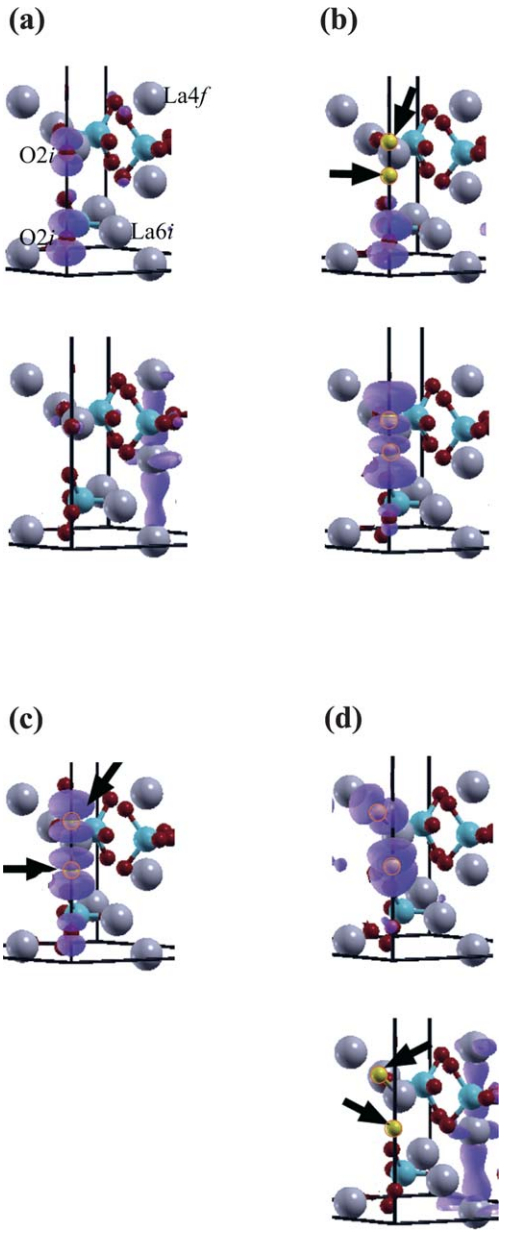

Fig. 7 The isosurface plot of the amplitude of the wave function of 0.1 $Å^{-3/2}$ of the highest occupied state (top panels) and the lowest unoccupied state (lower panels) for (a) the host and (b)–(d) oxygen-interstitial incorporated $La_{9.33}Si_6O_{26}$ in different charge states: neutral, −1, and −2, respectively. Note that the highest occupied and lowest unoccupied states are degenerate in the −1 charge defect-containing structure. Only atoms close to the oxygen interstitial are displayed. Oxygen split-interstitial pairs are indicated by arrows.

along the [001] direction. Similarly, La-5d is observed in the unoccupied state. These are indicated in the PDOS analysis in Fig. 3. From Fig. 7 (b), it can be seen that the unoccupied defect state of $O_i^{\times}$ has large amplitude in the interstitial region, indicating a pσ-like anti-bonding characteristic. In the charged states, there is clear evidence that the wave function from the occupied defect level remains localized at the oxygen interstitial sites, and is characterized by an antibonding state, but these defect levels are located much lower in the gap, as shown in Fig. 6. The spatial orientation of the 2p orbitals of O''_i is significantly different: the defect level becomes more localized than that of O'_i.

3.3 Mechanism and energy barrier of oxygen interstitial migration

The diffusion path in the perfect crystal can be defined by the change in atomic positions between two configurations which are equivalent in symmetry, but separated by some distance. Although no symmetry will exist in the real $La_{9.33}Si_6O_{26}$ material due to the random distribution of V_{La}s, the model for this distribution in the present study causes $P6_3$ symmetry in the supercell. For example, the points (x, y, z) and $(y, -x + y, z + 3/2)$ are equivalent. Thus, the diffusion path between these points was investigated. It should be noted that there are semi-equivalent configurations along the path: If V_{La} did not exist, there would be more equivalent points, which would be separated by $(1/2)c$ along the [001] direction with three-fold rotational symmetry.

Fig. 8 is the potential energy profile of oxygen interstitial migration in different charged states, calculated using the present structural model. It can be seen that O''_i, which is the most stable in a wide range of E_F, has a bumpy profile. We found that there are metastable configurations along the path, corresponding to the semi-equivalent points described above. The split interstitial pairs for these are centered at (0.03725, 0.00485, 1.2402) and (−0.0362, −0.00225, 1.74795). We denote the most stable configuration and its nearest equivalent as A and A′, respectively, and the semi-equivalent states as B and C. The metastable configuration B in the figure was found by the full relaxation of the atoms, although the potential energy profile exhibits no local minimum at B due to the coarse mesh in the NEB diffusion path search. Moreover, another metastable configuration was added between the A and B configurations. Except for this additional metastable configuration, the other three configurations are very similar: the split interstitial is located at the original O 2*a* sites.

The highest energy in the present energy profile for the double-negatively charged state was found between configurations C and A′, and the migration barrier, or the energy measured from the potential of A, is 0.58 eV. Although the real V_{La} distribution will deviate from that of the present model, the results indicate that V_{La} creates an energy difference between the configurations from −0.26 to 0.11 eV, measured from that of B, modulating the potential energy profile between sites. It can be expressed as a sum of the linear energy change between the sites and a primitive energy barrier of 0.15–0.3 eV. Assuming that the highest energy along the path is associated with configuration C and a half of the maximum primitive energy barrier, it will be 0.11 + 0.15 eV measured from B, resulting in a migration barrier of 0.52 eV from configuration A. The reported activation energies of ionic conductivity in $La_{9.33}Si_6O_{26}$, based on impedance measurements, are distributed in the range of 0.51–0.80 eV.[25–27] Despite the simplicity of the model, the calculation values did fall within this range.

The present calculations demonstrate that an atomic configuration change between A and B occurs as follows: One of the split interstitial pairs of atoms migrates to the original 2*a* site. At the same time, the other atom approaches the adjacent O atom at the 2*a* site to form a new pair. Due to the slanted geometry of the pair, the migrating oxygen interstitial pair adopts a simultaneous rotation. The changes from B to C and from C to the adjacent A occur in the same manner.

The migration mechanism of O''_i proposed by Béchade *et al.*[9] is very similar to the present one, as is the most stable geometry. Nevertheless, the migration barrier obtained here is about 0.21 eV higher than their result. The difference in the present theory is the explicit consideration of the effects of V_{La} and the use of the total energy theory. Interestingly, their calculated migration barrier was similar to the barrier height estimated in above analysis between the stable and metastable sites. It follows that V_{La} enhances the migration barrier.

Similar migration paths were found for other charged states. The metastable B and C configurations in the split pair were found at the original O 2*a* sites, configured parallel to the *c*-axis as in the most stable configuration of $O_i^{\times}$ and O'_i. The change in the split pair position occurred in a similar manner to that of O''_i, but the atomic movements are confined to straight lines. The energy barrier for the whole migration path of $O_i^{\times}$ was estimated to be 0.85 eV. In the charged O'_i migration path, the interstitial pair migrates *via* a similar transient configuration to that of the neutral case, except the interatomic distance between the two interstitial atoms is larger. This path was estimated to have a much lower migration energy of 0.38 eV than the uncharged case.

The energy profiles, especially, for the $O_i^{\times}$ state, are rather simple. This might be because oxygen moves only on the *c*-axis, or the lower charge of O_i might have been less affected by V_{La}. In fact, the energy difference between the stable and metastable configurations is less than 0.2 eV. On the other hand, for the O''_i migration, when La and V_{La} at the 4*f* sites are replaced by other combinations of elements with smaller charge differences, a change in the energy differences between the stable and metastable configurations would be expected. Unfortunately, the current experimental data are scattered over a rather wide range, making comparison difficult.

The calculated formation enthalpies and migration barriers can be combined to yield the oxygen activation energies as a function of the Fermi level when the system is attached to a reservoir. These results are shown in Fig. 5 (b). The overall features closely resembles those of the formation enthalpies, but O'_i becomes energetically stable in a narrow range of the Fermi level.

While the present lanthanum compounds are known to exhibit an interstitial or interstitialcy mechanism of oxygen diffusion, the vacancy mechanism is very popular in many oxides. We also estimated the energy change along a part of the migration path of the oxygen vacancy in the double-positively charged state. We observed 1.16 (forward) and 1.24 (backward) eV along the *z* direction, which is much higher than that of the interstitialcy mechanism.

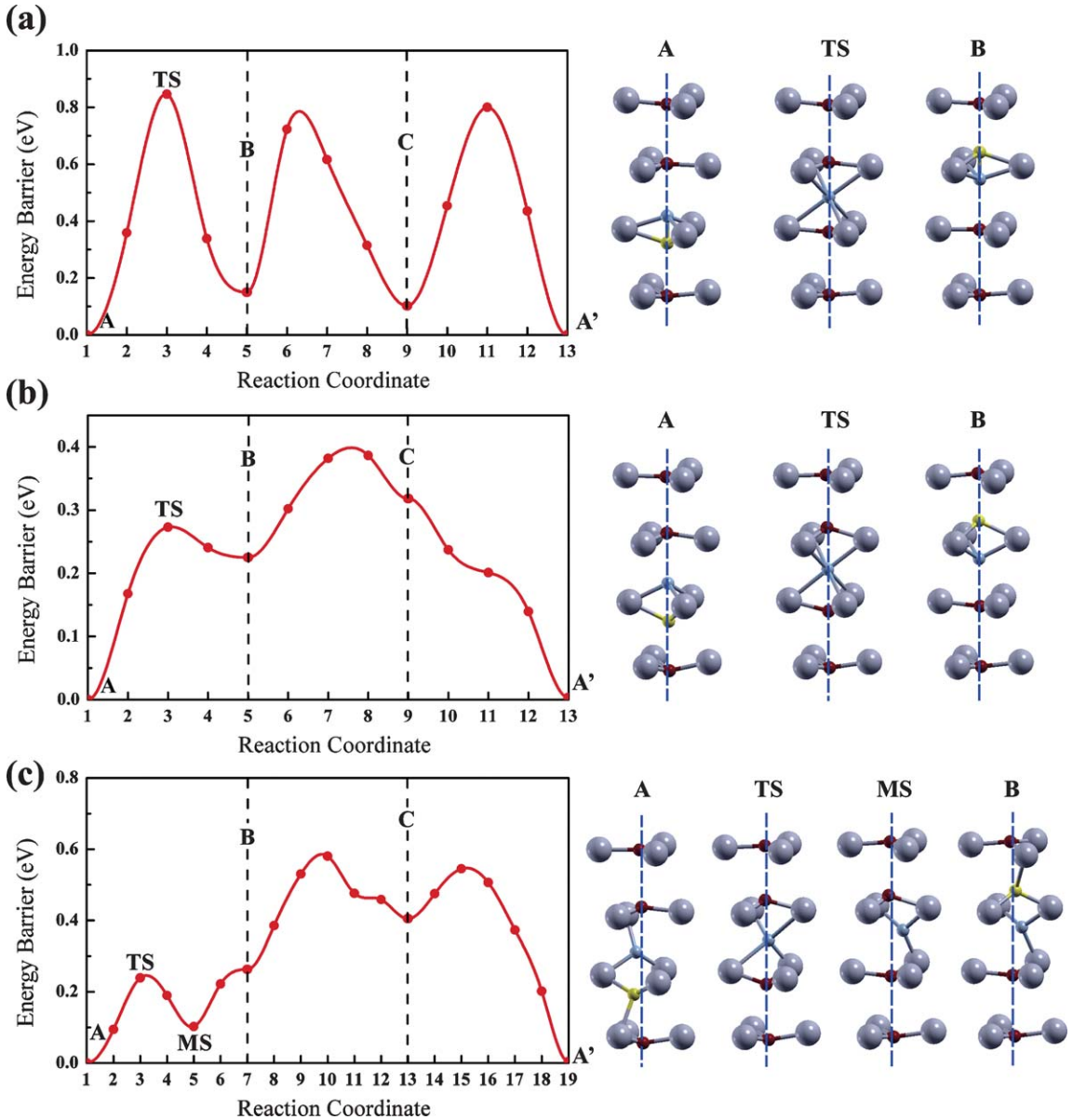

Fig. 8 Potential energy profiles of the oxygen interstitial diffusion path between equivalent coordination in excess-oxygen $La_{9.33}Si_6O_{26}$ with different charge states: (a) neutral, (b) −1, and (c) −2. The metastable intermediate state is denoted by the broken line. The changes in the local atomic configurations of the conduction channel in the starting, intermediate, and ending images denoted in the left panel are also illustrated in the right: the yellow balls symbolize the inserted oxygen interstitial and the blue balls indicate the moving transition oxygen atoms. The atomic configurations obtained for state C are similar to those of states A and B.

The Arrhenius-type temperature change of the diffusion constants has often been interpreted as indicating a thermal formation of the defect and thermal diffusion. The calculated migration barrier height is close to the experimental activation energy. Furthermore, the formation enthalpy of the oxygen Frenkel pair is much larger, as described above. Thus, the present calculations suggest that the excess oxygen has an extrinsic origin.

4. Conclusions

This work provides the first theoretical determination of the position preference, formation enthalpies, and migration barrier of O interstitial ions in $La_{9.33}Si_6O_{26}$ within the DFT using the supercell method. Special attention was given to structural exploration, electronic structure analysis, and the effects of the charge state. The V_{La} distribution was modeled in the supercell and determined to be the energetically favorable state. It was then used as the equilibrium structure for electronic structure analysis. We obtained 4.87 eV as the density-functional energy band gap. We also studied the chemical bonding in $La_{9.33}Si_6O_{26}$, and provided a picture of the electronic structure of this apatite-structured material.

Different stable atomic configurations were recognized for excess-oxygen $La_{9.33}Si_6O_{26}$, depending on the charge state.

A split O interstitial pair was formed by pushing an O atom in the 2*a* Wyckoff position away from its normal site by an inserted O atom, and was aligned along the [001] direction for the neutral and −1 charged interstitials, or with the midpoint of the split pair deviating from the channel center and pointed in the [012] direction in the −2 charged case. For a possible Fermi level range, the oxygen interstitial in its full formal charge states, O''_i, is in predominance, with an additional contribution from $O_i^{\times}$. This stable atomic configuration proposed for O''_i is very close to that obtained in previous atomistic simulations. In all three excess-oxygen $La_{9.33}Si_6O_{26}$ models, the O interstitial introduce gap state which largely distributes in the O interstitial pair site in real space, showing a pσ-like anti-bonding characteristic.

For interstitial-mediated diffusion in $La_{9.33}Si_6O_{26}$, we found that the calculated migration energies were small and had charge-dependent characteristics: 0.85 eV for $O_i^{\times}$, 0.38 eV for O'_i, and 0.58 eV for O''_i. In spite of the similarity of the atomic configuration to that found in a previous study, the barrier height of O''_i was higher due to the strong effects of V_{La}. These results support the idea that O interstitials are quite mobile in the ionic conductor $La_{9.33}Si_6O_{26}$. Our calculated diffusion barriers are in agreement with previously reported experimental values. Furthermore, the sensitivity of the local potential energy of an oxygen interstitial, especially a charged one, in response to the distance to a preexisting V_{La} cannot be ignored.

Acknowledgements

We are grateful to Dr Kiyoshi Kobayashi for fruitful discussions and for providing experimental data. We also thank Dr Guido Roma for his kind discussion of theoretical calculations. The numerical calculations were performed using the Numerical Materials Simulator in NIMS. This research was partly supported by Grant-in-Aid for Scientific Research (C) (No. 22560663) from the Japan Society for the Promotion of Science and the MEXT Program for the Development of Environmental Technology using Nanotechnology.

References

1 (*a*) O. Yamamoto, *Electrochim. Acta*, 2000, **45**, 2423–2435; (*b*) B. C. H. Steele, *J. Mater. Sci.*, 2001, **36**, 1053–1068; (*c*) V. V. Kharton, F. M. B. Marques and A. Atkinson, *Solid State Ionics*, 2004, **174**, 135–149.
2 (*a*) Y. Mishima, H. Mitsuyasu, M. Ohtaki and K. Eguchi, *J. Electrochem. Soc.*, 1998, **145**, 1004–1007; (*b*) J. P. P. Huijsmans, F. P. F. van Berkel and G. M. Christie, *J. Power Sources*, 1998, **71**, 107–110; (*c*) K. Q. Huang and J. B. Goodenough, *J. Alloys Compd.*, 2000, **303–304**, 454–464; (*d*) H. Yoshioka and S. Tanase, *Solid State Ionics*, 2005, **176**, 2395–2398; (*e*) P. R. Slater, J. E. H. Sansom and J. R. Tolchard, *Chem. Rec.*, 2004, **4**, 373–384.
3 (*a*) S. Nakayama, H. Aono and Y. Sadaoka, *Chem. Lett.*, 1995, **24**, 431–432; (*b*) S. Nakayama, H. A. T. Kagayama and Y. Sadaoka, *J. Mater. Chem.*, 1995, **5**, 1801–1805; (*c*) S. Nakayama and M. Sakamoto, *J. Eur. Ceram. Soc.*, 1998, **18**, 1413–1418; (*d*) K. Kuroda, I. Hashimoto, K. Adachi, J. Akikusa, Y. Tamou, N. Komada, T. Ishihara and Y. Takita, *Solid State Ionics*, 2000, **132**, 199–208; (*e*) A. L. Shaula, V. V. Kharton and F. M. B. Marques, *J. Solid State Chem.*, 2005, **178**, 2050–2061.
4 D. Marrero-López, M. C. Martín-Sedeño, J. Peña-Martínez, J. C. Ruiz-Morales, P. Núñez, M. A. G. Aranda and J. R. Ramos-Barrado, *J. Power Sources*, 2010, **195**, 2496–2506.
5 H. Okudera, Y. Masubuchi, S. Kikkawa and A. Yoshiasa, *Solid State Ionics*, 2005, **176**, 1473–1478.
6 Y. Matsushita, F. Izumi, K. Kobayashi, N. Igawa, H. Kitazawa, Y. Oyama, S. Miyoshi and S. Yamaguchi, *Nucl. Instrum. Methods Phys. Res., Sect. A*, 2009, **600**, 319–321.
7 (*a*) S. W. Tao and J. T. S. Irvine, *Mater. Res. Bull.*, 2001, **36**, 1245–1258; (*b*) S. S. Pramana, W. T. Klooster and T. J. White, *Acta Crystallogr., Sect. B: Struct. Sci.*, 2007, **63**, 597–602; (*c*) L. León-Reina, E. R. Losilla, M. Martinez-Lara, S. Bruque, A. Llobet, D. V. Sheptyakov and M. A. G. Aranda, *J. Mater. Chem.*, 2005, **15**, 2489–2498.
8 J. R. Tolchard, M. S. Islam and P. R. Slater, *J. Mater. Chem.*, 2003, **13**, 1956–1961.
9 E. Béchade, O. Masson, T. Iwata, I. Julien, K. Fukuda, P. Thomas and E. Champion, *Chem. Mater.*, 2009, **21**, 2508–2517.
10 J. P. Perdew, K. Burke and M. Ernzerhof, *Phys. Rev. Lett.*, 1996, **77**, 3865–3868.
11 D. Vanderbilt, *Phys. Rev. B: Condens. Matter*, 1990, **41**, 7892–7895.
12 J. D. Pack and H. J. Monkhorst, *Phys. Rev. B: Solid State*, 1977, **16**, 1748–1749.
13 S. Baroni, A. D. Corso, S. de Gironcoli, P. Giannozzi, PWSCF (plane wave self consistent field codes), available at: http://www.quantum-espresso.org.
14 S. B. Zhang and J. E. Northrup, *Phys. Rev. Lett.*, 1991, **67**, 2339–2342.
15 G. Henkelman, B. P. Uberuaga and H. Jonsson, *J. Chem. Phys.*, 2000, **113**, 9901–9904.
16 L. Wang, T. Maxisch and G. Ceder, *Phys. Rev. B*, 2006, **73**, 195107-1–10.
17 T. Iwata, K. Fukuda, E. Béchade, O. Masson, I. Julien, E. Champion and P. Thomas, *Solid State Ionics*, 2007, **178**, 1523–1529.
18 L. León-Reina, J. M. Porras-Vázquez, E. R. Losilla, D. V. Sheptyakov, A. Llobet and M. A. G. Aranda, *Dalton Trans.*, 2007, 2058–2064.
19 J. E. H. Sansom, D. Richings and P. R. Slater, *Solid State Ionics*, 2001, **139**, 205–210.
20 M. S. Islam, J. R. Tolchard and P. R. Slater, *Chem. Commun.*, 2003, 1486–1487.
21 A. S. Risbud, K. B. Helean, M. C. Wilding, P. Lu and A. Navrotsky, *J. Mater. Res.*, 2001, **16**, 2780–2783.
22 F. Detraux, F. Finocchi and X. Gonze, *Phys. Rev. B: Condens. Matter Mater. Phys.*, 2006, **73**, 165208.
23 A. Kuwabara and I. Tanaka, *J. Phys. Chem. B*, 2004, **108**, 9168–9172.
24 C. G. Van de Walle and J. Neugebauer, *J. Appl. Phys.*, 2004, **95**, 3851–3879.
25 C. Y. Ma, P. Briois, J. Böhlmark, F. Lapostolle and A. Billard, *Ionics*, 2008, **14**, 471–476.
26 J. E. H. Sansom, A. Najib and P. R. Slater, *Solid State Ionics*, 2004, **175**, 353–355.
27 C. Bonhomme, S. Beaudet-Savignat, T. Chartier, A. Maître, A. L. Sauvet and B. Soulestin, *Solid State Ionics*, 2009, **180**, 1593–1598.

